Journal of
MATERIALS RESEARCH

Welcome Comments Help

Momentum and thermal boundary-layer thickness in a stagnation flow chemical vapor deposition reactor

David S. Dandy and Jungheum Yun
Department of Chemical Engineering, Colorado State University, Fort Collins, Colorado 80523-1370

(Received 25 March 1996; accepted 21 October 1996)

Explicit expressions have been derived for momentum and thermal boundary-layer thickness of the laminar, uniform stagnation flows characteristic of highly convective chemical vapor deposition pedestal reactors. Expressions for the velocity and temperature profiles within the boundary layers have also been obtained. The results indicate that, to leading order, the momentum boundary-layer thickness is inversely proportional to the square root of the Reynolds number, while the thermal boundary-layer thickness is inversely proportional to the square root of the Peclet number. Values computed using the approximate expressions are compared directly with numerical solutions of the equations of motion and thermal energy equation, for a specific set of conditions typical of diamond chemical vapor deposition. Because values of the Lewis number do not vary significantly from unity for many different chemical vapor deposition systems, the expression derived here for thermal boundary-layer thickness may be used directly as an approximate concentration boundary-layer thickness.

I. INTRODUCTION

Chemical-vapor-deposited (CVD) diamond is grown in a variety of environments using many different techniques.[1,2] Of the high growth rate deposition technologies for the synthesis of diamond via low-pressure chemical vapor deposition, direct current (dc) arcjet reactor systems[3–8] have proven to be reliable for the production of high quality, relatively large area films.[9–12] In this type of reactor, high growth rates result from very large fluxes of materials passing through the plasma gun and impinging upon the substrate, and a uniform gas-phase environment and deposition over a large surface area result from the stagnation flow occurring in this type of reactor.[2] A number of specific models have been developed for idealized straining flow,[4] stagnation flow,[2] and one-dimensional boundary layers[13] in dc arcjet reactors. These models are all based upon solution of the coupled momentum, energy, and species mass conservation equations, subject to the geometric constraints appropriate for each reactor type.

While the theoretical treatment of transport and chemical kinetics in the dc arcjet reactors is rigorous,[2,4,12–15] the models are generally very complex and computer intensive; further the ability to obtain a converged numerical solution is often sensitive to not only the operating conditions specified, but also to the initial condition used in the iterative solution technique. These models can require anywhere from tens of minutes to several hours to successfully execute, and consequently are difficult to incorporate directly into intelligent process control design algorithms.[12]

Experience gained from using detailed stagnation flow models to analyze film growth in dc arcjet systems has provided necessary insight for the development of simplified analytical models for diamond deposition.[12,15] These analytical models are used to predict gas-phase species distributions, diamond growth rate, and heat flux to the substrate; however, to calculate mass and energy fluxes at the substrate, the models require estimates of the boundary-layer thickness, which in turn are dependent upon multicomponent transport properties. The boundary-layer thickness falls out naturally from the detailed model results, but since the analytical models are, in some sense, intended to replace the detailed models, it is necessary to have *a priori* estimates of boundary-layer thickness.

By exploiting the idealized stagnation flow conditions present in many dc arcjet reactors, it is possible to derive approximate expressions for boundary-layer thickness using the Karman–Pohlhausen method. In the following sections this method will be applied to a general, uniform stagnation flow in order to develop analytical expressions for momentum and thermal boundary-layer thickness as functions of effective Reynolds number and Prandtl number. The results of this work will be compared against detailed stagnation flow calculations,[2,12] using conditions applicable to diamond growth. It is important to recognize that, while the actual numbers to be presented here are specific to the diamond reactor environment, the analytical results are valid for any system with laminar, uniform stagnation flow at high Reynolds number.

II. PROBLEM FORMULATION

Consider a dc arc plasma torch reactor configured with the axis of the plasma-torch orthogonal to the deposition surface[3,4,9,16] such that the hot, high-velocity gas jet issuing from the orifice of the torch produces an axisymmetric flow field when it impinges upon the temperature-controlled substrate, as illustrated schematically in Fig. 1. The gas experiences a 5 : 1 to 20 : 1 pressure drop as it flows through the torch orifice, passing through a normal shock and spreading rapidly into the low-pressure reactor environment (5–100 Torr, typically), and producing a fairly uniform axial laminar flow within 0.5 cm of the torch exit. In this work attention is focused on forced convection transport in the region between the torch exit and the substrate. It is assumed that the flow in this region can be approximated by a uniform stagnation flow, as illustrated in Fig. 2.[2] Although the gas does have a swirl component as it leaves the torch and the substrate usually rotates (to ensure azimuthal film uniformity), the swirl and spin Reynolds numbers are up to two orders of magnitude lower than the forced convection, or stagnation, Reynolds number, which will attain values of over 800 for the conditions to be considered here.

Since the flow is laminar and Reynolds number lies in the range $500 \leqslant Re \leqslant 2000$, the flow behaves as if it were nearly inviscid over most of the domain, with viscous and diffusive effects only becoming important in a thin region near the substrate. In other words there are true momentum and thermal boundary layers present, with thickness denoted by δ and δ_T, respectively, such that δ, $\delta_T \ll L$. Within the boundary layer, the velocity rapidly decreases from its potential flow value to zero at the surface, and the temperature decreases from its free stream value to that of the temperature-controlled substrate. Thus, the relevant transport length scale at the substrate is not directly dependent upon reactor dimension, but by an inherent length scale of the boundary layer thickness where the effects of diffusive transport are significant.[15]

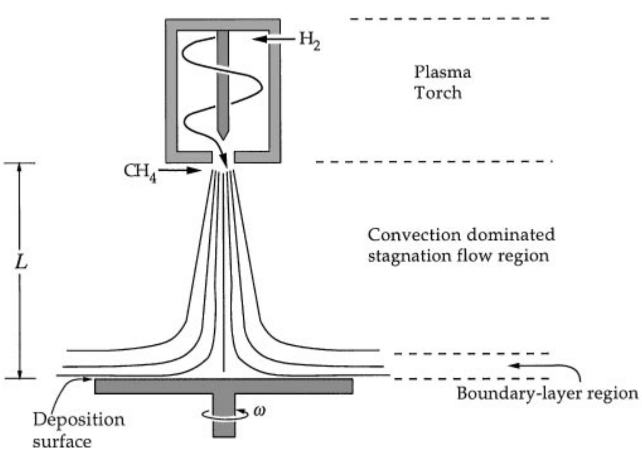

FIG. 1. Schematic diagram of the stagnation flow geometry in a typical dc arcject reactor.

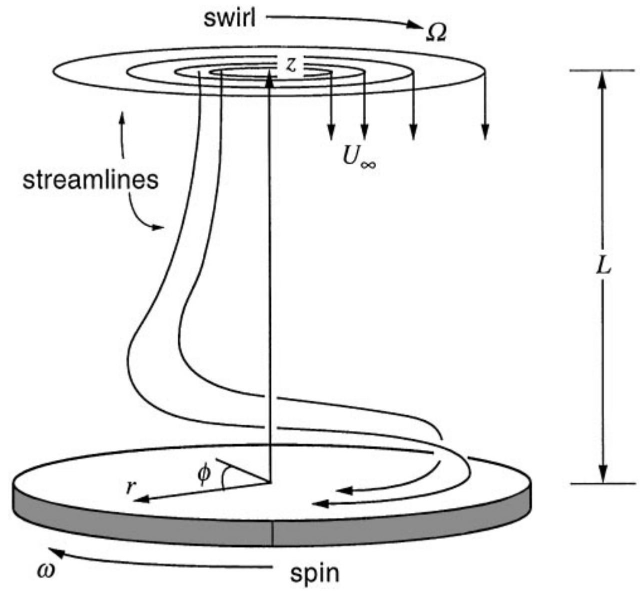

FIG. 2. Uniform stagnation flow field assumed to be present in the region between the plasma torch exit and the substrate. The cylindrical coordinates (r, ϕ, z) are used to describe the geometry of this system.

By making suitable assumptions regarding the nature of the stagnation flow and using an appropriate similarity transform, the equations describing this nonisothermal, reacting system can be reduced from a set of three-dimensional partial differential equations to a set of coupled ordinary equations. The methodology for using the similarity transform has been discussed by a number of investigators,[17–23] and therefore the details of this will not be presented here.

As a simplified example, however, consider a semi-infinite fluid above a rotating infinite disk.[20] The system is described in cylindrical polar coordinates (r, ϕ, z), with the infinite radius disk in the plane $z = 0$ and the fluid occupying the region $z > 0$. The rotation of the disk results in a secondary, downward axial flow, such that the fluid's velocity profile is three-dimensional, with components (u, ν, w). Recognizing that, for a viscous, semi-infinite fluid, the zone of influence of the disk is proportional to $\sqrt{\nu/\omega}$, a dimensionless similarity variable X can be defined such that $X = z\sqrt{\omega/\nu}$. The three components of the Navier–Stokes equations are then reduced to a set of ordinary, nonlinear differential equations in a single independent variable, X. It is assumed that the dependent variables are separable functions of the radial and axial coordinates. Specifically, the axial velocity and temperature are functions of the axial coordinate only, and the radial and circumferential velocities and the radial pressure gradient depend linearly on the radial coordinate. The similarity transforms for the dependent variables take the form

$$u = r\omega F(X),$$
$$v = r\omega G(X),$$
$$w = \sqrt{\nu\omega} H(X),$$
$$p/\rho = \nu\omega p_0(X) + \frac{1}{2}\kappa\omega^2 r^2,$$

where κ is a constant and F, G, H, and p_0 are the dimensionless functions to be determined. The resulting differential equations for the dimensionless unknowns are then

$$F'' = F^2 - G^2 + HF' + \kappa,$$
$$G'' = 2FG + HG',$$
$$p_0' = H'' - HH',$$
$$2F + H' = 0,$$

where the prime denotes differentiation with respect to X. These equations can then be solved numerically subject to suitable boundary conditions at $X = 0$ and $X \to \infty$.[20]

This similarity transform approach has been extended to the case of a forced, nonisothermal flow, with a finite boundary located at $z = L$,[23] which is the case to be considered here. In that study, results obtained using a similarity transformation similar to that above, but based on both disk rotation ω and forced convection U_∞, and these were compared directly against numerical solutions of the three-dimensional momentum and energy conservation equations. It was found that, over a wide range of rotation and stagnation Reynolds numbers, the similarity transform accurately predicted the velocity and temperature fields in the domain. This similarity approach has been employed to study a number of stagnation flow reactors[2,13,24–26] and forms the basis of a Fortran code called SPIN.[24]

To utilize the idealized stagnation flow field to develop approximate expressions for the boundary-layer thickness, it is necessary to make several simplifying assumptions.

(1) The velocity, temperature, and composition are known at the exit of the torch. The uniform axial down flow at the plasma-torch exit, located at the position $z = L$, is given by $-U_\infty$, and the temperature and chemical composition (mass fractions) are denoted by T_∞ and $Y_{k\infty}$.

(2) Plasma effects (charged species) are neglected; the fluid issuing from the torch is treated as a neutral gas[27,28] with a single thermodynamic temperature at the plasma-torch exit.

(3) The substrate is considered a plane with infinite radius so that edge effects may be neglected.

(4) The radial component of the velocity, u, at the surface must vanish due to the no-slip condition. Although the axial velocity component, w, is nonzero, at the surface due to the net flux of mass to the surface,[2] it can be ignored because $w|_{z=0} \ll U_\infty$. (In fact, the axial velocity at the surface is typically seven or eight orders of magnitude smaller than U_∞.)

(5) At the deposition surface the gas-phase temperature matches that of the substrate temperature T_s.

(6) While the system is nonisothermal, the temperatures remains nearly constant at T_∞ in the free stream, and drops almost linearly to T_s across the boundary layer. Figure 3 illustrates a typical temperature profile computed using SPIN,[24] for a reacting mixture of 0.5% methane in hydrogen at 20 Torr, and an average exit velocity $U_\infty = 2 \times 10^5$ cm/s. To characterize the transport behavior in the system, it is assumed that mixture properties such as density (ρ), viscosity (μ), and thermal conductivity (k) will be evaluated at the system pressure, p, and an effective, or average, temperature $T_{\text{eff}} = 1/2\ (T_s + T_\infty)$. It is also assumed that radiation heat transfer is secondary to convection heat transfer in the free stream.

(7) Disk and swirl Reynolds numbers ($L^2\omega/\nu$ and $L^2\Omega/\nu$) are small relative to the stagnation Reynolds number (LU_∞/ν), so forced convection alone is to be considered.

III. MOMENTUM TRANSPORT

If fluid properties are evaluated at T_{eff}, the r-component of the momentum equations and the con-

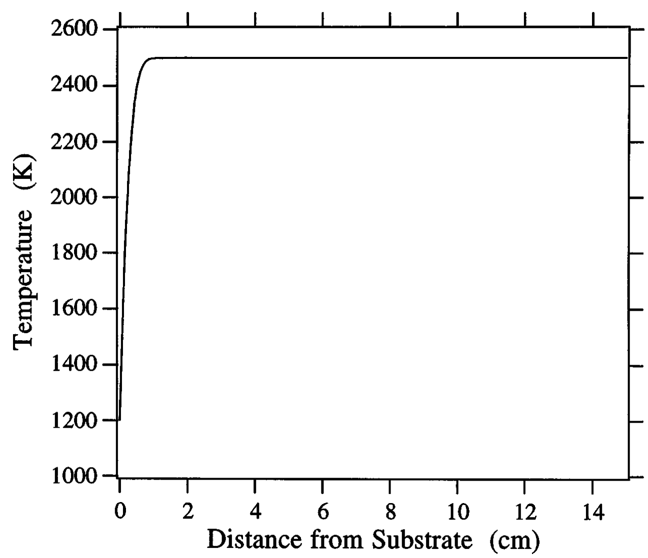

FIG. 3. Representative temperature profile computed by numerical solution of the equations of motion and thermal energy equation for $p = 20$ Torr and $U_\infty = 2 \times 10^5$ cm/s.

tinuity equation in the cylindrical coordinate system are

$$\rho\left(u\frac{\partial u}{\partial r}+w\frac{\partial u}{\partial z}\right)=-\frac{\partial p}{\partial r}+\mu\left[\frac{\partial^2 u}{\partial r^2}+\frac{\partial}{\partial r}\left(\frac{u}{r}\right)+\frac{\partial^2 u}{\partial z^2}\right], \tag{1}$$

and

$$\frac{\partial u}{\partial r}+\frac{u}{r}+\frac{\partial w}{\partial z}=0, \tag{2}$$

where u and w are the radial and axial velocity components, and all terms involving $\partial/\partial\phi$ have been dropped because of axial symmetry.

In order to nondimensionalize Eqs. (1) and (2), the characteristic length is chosen to be L, the characteristic velocity is U_∞, and the characteristic pressure is ρU_∞^2. Using these scales the dimensionless independent and dependent variables are denoted by

$$\tilde{r}=\frac{r}{L}\quad \tilde{x}=\frac{z}{L}\quad \tilde{p}=\frac{p}{\rho U_\infty^2} \tag{3}$$

$$\tilde{u}=\frac{u}{U_\infty}\quad \tilde{w}=\frac{w}{U_\infty}, \tag{4}$$

and the dimensionless governing equations are then

$$\tilde{u}\frac{\partial \tilde{u}}{\partial \tilde{r}}+\tilde{w}\frac{\partial \tilde{u}}{\partial \tilde{x}}=-\frac{\partial \tilde{p}}{\partial \tilde{r}}+\frac{1}{Re}\left[\frac{\partial^2 \tilde{u}}{\partial \tilde{r}^2}+\frac{\partial}{\partial \tilde{r}}\left(\frac{\tilde{u}}{\tilde{r}}\right)+\frac{\partial^2 \tilde{u}}{\partial \tilde{x}^2}\right], \tag{5}$$

$$\frac{\partial \tilde{u}}{\partial \tilde{r}}+\frac{\tilde{u}}{\tilde{r}}+\frac{\partial \tilde{w}}{\partial \tilde{x}}=0. \tag{6}$$

where the Reynolds number is $Re = LU_\infty/\nu$.

The domain consists of two distinct regions, a potential flow region encompassing almost the entire domain $0 < z \leqslant L$, and a momentum boundary-layer region $z \to 0$ where viscous effects must be considered. The two different flow regions are illustrated by the velocity profiles shown in Fig. 4, which were computed using SPIN with the conditions listed for Fig. 3. The modified radial velocity (u/r) increases monotonically due to continuity as the nearly inviscid flow approaches the disk, reaching a maximum at a distance proportional to $\sqrt{\nu/U_\infty}$. It then decreases in magnitude through the boundary layer and goes to zero at the substrate because of the no-slip condition. The axial velocity decreases monotonically over the entire domain, such that its magnitude in the boundary layer, that is, the region $z < O(\sqrt{\nu/U_\infty})$, is almost two orders of magnitude less than U_∞.

In terms of the governing equations, since the Reynolds number is large, $Re = O(10^3)$, in the potential flow region where L is the appropriate length scale the

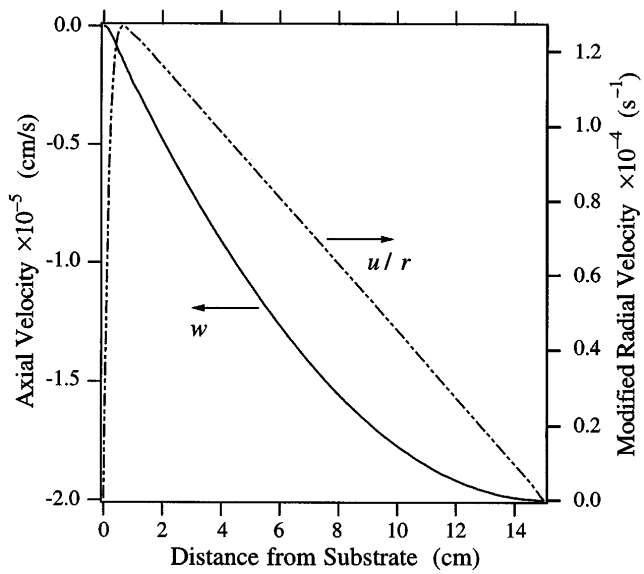

FIG. 4. Axial and modified radial velocity profiles for conditions corresponding to Fig. 3.

viscous terms in the dimensionless r-component become negligible relative to the inertial and pressure gradient terms. Thus, in the potential flow region the relevant equations are

$$\frac{\partial \tilde{u}}{\partial \tilde{r}}+\frac{\tilde{u}}{\tilde{r}}+\frac{\partial \tilde{w}}{\partial \tilde{x}}=0, \tag{7}$$

$$\tilde{u}\frac{\partial \tilde{u}}{\partial \tilde{r}}+\tilde{w}\frac{\partial \tilde{u}}{\partial \tilde{x}}=-\frac{\partial \tilde{p}}{\partial \tilde{r}}, \tag{8}$$

subject to the following boundary conditions:

$$\tilde{u}=0,\quad \tilde{w}=-1\qquad \text{at } \tilde{x}=1. \tag{9}$$

In order to capture the viscous effects present in the boundary layer, it is necessary to rescale the terms in the governing equations. Recognizing that vicious effects decelerate the modified radial velocity over a distance proportional to $\sqrt{\nu/U_\infty}$, the scaling is chosen to be

$$X = Re^{1/2}\tilde{x},\qquad W = Re^{1/2}\tilde{w}.$$

The governing equations in the boundary-layer region become

$$\frac{\partial \tilde{u}}{\partial \tilde{r}}+\frac{\tilde{u}}{\tilde{r}}+\frac{\partial W}{\partial X}=0 \tag{10}$$

and

$$\begin{aligned}\tilde{u}\frac{\partial \tilde{u}}{\partial \tilde{r}}+W\frac{\partial \tilde{u}}{\partial X}&=-\frac{\partial \tilde{p}}{\partial \tilde{r}}+\frac{1}{Re}\left[\frac{\partial^2 \tilde{u}}{\partial \tilde{r}^2}+\frac{\partial}{\partial \tilde{r}}\left(\frac{\tilde{u}}{\tilde{r}}\right)\right]+\frac{\partial^2 \tilde{u}}{\partial X^2}\\&=-\frac{\partial \tilde{p}}{\partial \tilde{r}}+\frac{\partial^2 \tilde{u}}{\partial X^2}+O(Re^{-1}).\end{aligned} \tag{11}$$

For this stagnation flow problem, the separability assumption applies, namely that $w = w(\tilde{x})$ and $\tilde{u}(\tilde{r}, \tilde{x}) = \tilde{r}\hat{u}(\tilde{x})$ in the potential, or outer domain, and $W = W(X)$ and $\tilde{u}(\tilde{r}, X) = \tilde{r}\hat{u}(X)$ in the boundary layer, or inner domain. When these definitions are substituted into Eqs. (7), (8), (10), and (11), the system is reduced to a set of ordinary differential equations:

$$2\tilde{u}_{FS} + \frac{d\tilde{w}}{d\tilde{x}} = 0 \tag{12}$$

$$\hat{u}_{FS}^2 + \tilde{w}\,\frac{d\hat{u}_{FS}}{d\tilde{x}} = -\frac{1}{\tilde{r}}\,\frac{\partial\tilde{p}}{\partial\tilde{r}} \tag{13}$$

in the outer region, and

$$2\hat{u}_{BL} + \frac{dW}{dX} = 0 \tag{14}$$

$$\hat{u}_{BL}^2 + W\,\frac{d\hat{u}_{BL}}{dX} = -\frac{1}{\tilde{r}}\,\frac{\partial\tilde{p}}{\partial\tilde{r}} + \frac{d^2\hat{u}_{BL}}{dX^2} \tag{15}$$

in the inner region. In Eqs. (12)–(15) the subscripts FS and BL are attached to the modified radial velocity to distinguish that quantity between the outer and inner regions.

In order to apply the Karman–Pohlhausen method, approximate expressions for the velocity components must be determined. For the inner region it is assumed that $\tilde{u}$ can be expressed as a cubic polynomial in X:

$$\tilde{u}_{BL} = \tilde{r}(a + b\xi^2 + d\xi^3)\,. \tag{16}$$

Thus, the modified radial velocity can be expressed as

$$\hat{u}_{BL} = a + b\xi + c\xi^2 + d\xi^3\,, \tag{17}$$

where $\xi = X/\zeta$, and ζ is the (unknown) dimensionless momentum boundary-layer thickness; ζ is related to the dimensional boundary-layer thickness by $\zeta = Re^{1/2}\delta/L$. Four constraints on $\hat{u}_{BL}$ must be specified, and these are

$$\hat{u}_{BL} = 0\,, \quad \frac{d^2\hat{u}_{BL}}{d\xi^2} = 0 \qquad \text{at } \xi = 0\,, \tag{18}$$

$$\hat{u}_{BL} = \alpha\,, \quad \frac{d\hat{u}_{BL}}{d\xi} = 0 \qquad \text{at } \xi = 1\,. \tag{19}$$

The conditions at the surface arise from the no-slip condition and Eq. (15), while the conditions at the edge of the boundary layer are based upon the characteristics of the $\hat{u}$ profile shown in Fig. 4. The value of α is not known in advance and must be determined through matching with the outer solution. When the boundary conditions in Eqs. (18) and (19) are prescribed, the resulting expression for $\hat{u}_{BL}$ becomes

$$\hat{u}_{BL} = \frac{1}{2}\,\alpha\xi(3 - \xi^2)\,. \tag{20}$$

Then, substitution of Eq. (20) into the continuity equation, Eq. (14), and integration in ξ over the boundary layer, results in an expression for the axial velocity component:

$$W = -\alpha\zeta\xi^2\left(\frac{3}{2} - \frac{1}{4}\,\xi^2\right), \tag{21}$$

or, in terms of the unscaled variable,

$$\tilde{w}_{BL} = -(\delta/L)\alpha\xi^2\left(\frac{3}{2} - \frac{1}{4}\,\xi^2\right). \tag{22}$$

The value of the axial velocity at the outer edge of the boundary layer is then

$$\tilde{w}_{BL} = -\frac{5}{4}\,\frac{\delta}{L}\,\alpha \qquad \text{at } \xi = 1\,. \tag{23}$$

From inspection of Fig. 4, it is assumed that the modified radial velocity in the outer region in nearly linear in $\tilde{x}$, such that

$$\hat{u}_{FS} = a + b\tilde{x}\,. \tag{24}$$

The corresponding expression for the axial velocity component is then

$$\tilde{w}_{FS} = -2\tilde{x}\left(a + \frac{1}{2}\,b\tilde{x}\right) + c\,. \tag{25}$$

The constants a, b and c must be determined through boundary conditions at $\tilde{x} = 1$ and matching with the inner solution as $\tilde{x} \to 0$. Applying the conditions at the inlet,

$$\hat{u} = 0\,, \quad \tilde{w} = -1 \qquad \text{at } \tilde{x} = 1\,, \tag{26}$$

it is found that $b = -a$ and $c = a - 1$. Matching conditions are then applied in the area joining the inner and outer regions:

$$\begin{aligned} \lim_{X\to\infty} \hat{u}_{BL} &\longleftrightarrow \lim_{\tilde{x}\to 0} \hat{u}_{FS} \\ \lim_{X\to\infty} \hat{w}_{BL} &\longleftrightarrow \lim_{\tilde{x}\to\infty} \hat{w}_{FS}\,. \end{aligned} \tag{27}$$

Application of these two conditions yields two equations in two unknowns,

$$\alpha = a\left(1 - \frac{\delta}{L}\right) \tag{28}$$

and

$$-\frac{5}{4}\,\frac{\delta}{L}\,\alpha = -2a\frac{\delta}{L}\left(1 - \frac{1}{2}\,\frac{\delta}{L}\right) + a - 1\,. \tag{29}$$

The resulting expressions for a, b, and c are then

$$a = -b = \frac{4}{(4 + \delta/L)(1 - \delta/L)} \tag{30}$$

$$c = \frac{3 + \delta/L}{(4 + \delta/L)(1 - \delta/L)}\,\frac{\delta}{L}\,, \tag{31}$$

such that

$$\alpha = \frac{4L}{\delta + 4L}\,. \tag{32}$$

Using the four constants in (30)–(32), expressions for the velocity components in the outer and inner regions can now be written as

$$\hat{u}_{FS} = \frac{4(1 - \tilde{x})}{(4 + \delta/L)(1 - \delta/L)} \tag{33}$$

$$\tilde{w} = \frac{4(\tilde{x} - 1)^2}{(4 + \delta/L)(1 - \delta/L)} - 1 \tag{34}$$

$$\hat{u}_{BL} = \frac{2\xi(3 - \xi^2)}{4 + Re^{-1/2}\zeta} \tag{35}$$

and

$$W = -\frac{2\zeta\xi^2\left(3 - \frac{1}{2}\xi^2\right)}{4 + Re^{-1/2}\zeta}, \tag{36}$$

where the dimensional and dimensionless boundary-layer thickness are related by $\delta = L\zeta Re^{-1/2}$.

To illustrate the nature of the velocity components within the boundary layer and the matching of velocities between the two regions, a single case is considered corresponding to the conditions of Fig. 3, except that the pressure is 60 Torr rather than 20 Torr. For this case it has been determined that the dimensionless boundary-layer thickness is $\zeta = 1.38$, which corresponds to $\delta = 0.21$ cm. The potential flow components in Eqs. (33) and (34) are scaled appropriately, and plotted with the boundary-layer components of Eqs. (35) and (36) against the dimensionless boundary-layer coordinate, X, in Fig. 5.

The final quantity to be determined before applying the Karman–Pohlhausen method is the radial pressure gradient appearing in the rescaled boundary-layer equations. Because the axial component of the rescaled boundary-layer equations simplifies to

$$\frac{\partial \tilde{p}}{\partial X} = O(Re^{-1}), \tag{37}$$

it is possible to determine $\partial\tilde{p}/\partial\tilde{r}$ by evaluating the radial component of the equations at any axial position. For convenience this position is chosen to be the outer edge of the boundary layer, $\xi = 1$, because the necessary information is available from the potential flow solution. The resulting expression for the pressure gradient at any position $0 \leqslant X \leqslant \zeta$ is

$$-\frac{1}{\tilde{r}}\frac{d\tilde{p}}{d\tilde{r}} = \hat{u}_{FS}^2\Big|_{\xi=1} + \tilde{w}\,\frac{d\hat{u}_{FS}}{dX}\Big|_{\xi=1} = \alpha^2 = \frac{16}{(4 + Re^{-1/2}\zeta)^2} \tag{38}$$

Substituting this result into Eq. (15) yields

$$\hat{u}_{BL}^2 + W\frac{d\hat{u}_{BL}}{dX} = \frac{16}{(4 + Re^{1/2}\zeta)^2} + \frac{d^2\hat{u}_{BL}}{dX^2} \tag{39}$$

which serves as the starting point for the determination of the surface shear stress, τ_s, and the momentum boundary-layer thickness, δ. Carrying out the variable transformation $\xi = X/\zeta$ in Eq. (39), and subsequently integrating that equation across the boundary layer, an expression for the dimensionless shear stress at the surface is obtained:

$$-\frac{1}{\zeta}\frac{d\hat{u}_{BL}}{d\xi}\Big|_{\xi=0} = \int_0^1 \hat{u}_{BL}^2\zeta\,d\xi + \int_0^1 W\frac{d\hat{u}_{BL}}{d\xi}\,d\xi - \frac{16\zeta}{(4 + Re^{-1/2}\zeta)^2}. \tag{40}$$

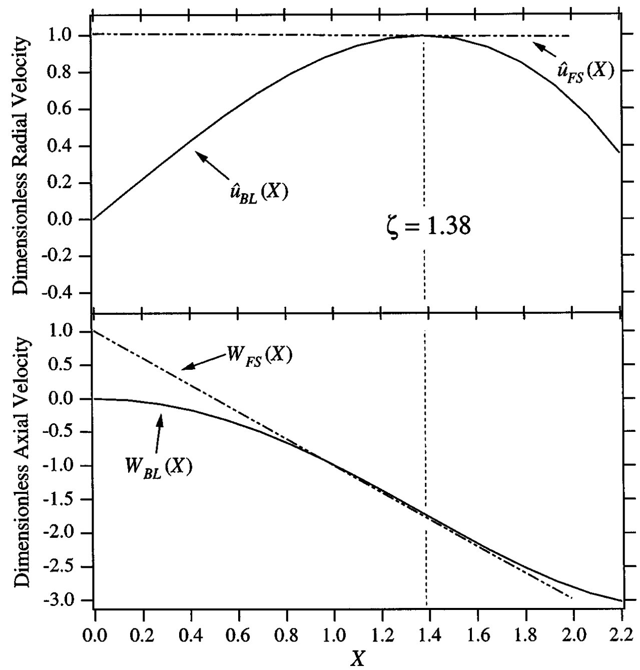

FIG. 5. Axial and modified radial velocity profiles in the matching region of the boundary-layer and potential flow solutions. The conditions used are $T_s = 1200$ K, $T_\infty = 2500$ K, $p = 60$ Torr, and $U_\infty = 2 \times 10^5$ cm/s.

Substituting the approximate expressions for $\hat{u}_{BL}$ and W, Eqs. (35) and (36), into Eq. (40) and then simplifying the result, a quadratic equation is obtained for the dimensionless momentum boundary-layer thickness, ζ, which yields a single physical root. In dimensional form, then, the momentum boundary-layer thickness is uniform stagnation flow is given approximately by

$$\delta = \frac{L}{Re^{1/2}}\left[\frac{0.2365}{Re^{1/2}} + \left(1.892 + \frac{0.0559}{Re}\right)^{1/2}\right]. \tag{41}$$

However, for values of the Reynolds number for which a boundary layer actually exists, $Re \geqslant O(10^2)$, the expression for ζ is dominated by a single term; and it is therefore a reasonable approximation to write

$$\delta \cong 1.375 L Re^{-1/2}. \tag{42}$$

The presumption that the viscous length scale is proportional to $\sqrt{\nu/U_\infty}$ is borne out by this result.

Using the approximate expression found for the radial velocity component in the boundary layer, the shear stress at the surface can be evaluated:

$$\tau_s = \mu \left.\frac{\partial u}{\partial z}\right|_{z=0} = \mu \frac{rU_\infty}{\delta L} \left.\frac{d\hat{u}}{d\xi}\right|_{\xi=0}$$
$$= 6\mu \frac{rU_\infty}{\delta L}\left(\frac{L}{\delta + 4L}\right). \qquad (43)$$

Assuming that Eq. (42) is valid, the expression for shear stress becomes

$$\tau_s = 4.36\mu \frac{rU_\infty}{L^2}\left(\frac{Re}{1.375 + 4Re^{1/2}}\right). \qquad (44)$$

Since the radial coordinate r is a monotonic function, the surface shear stress can never change sign, and as a result, it is predicted that boundary-layer separation cannot occur.

IV. ENERGY TRANSPORT

In this gaseous system, it's assumed that kinetic and potential energy changes, as well as viscous dissipation, contribute negligibly to the total energy balance. At steady state, utilizing the assumption that fluid properties are evaluated at an effective temperature T_{eff}, the axisymmetric form of thermal energy equation in cylindrical coordinates is

$$\rho\hat{C}_p\left(u\frac{\partial T}{\partial r} + w\frac{\partial T}{\partial z}\right) = k\left[\frac{1}{r}\frac{\partial}{\partial r}\left(r\frac{\partial T}{\partial r}\right) + \frac{\partial^2 T}{\partial z^2}\right], \qquad (45)$$

where $\hat{C}_p$ and k are the mixture specific heat capacity and thermal conductivity, respectively. To nondimensionalize this equation the characteristic length and velocity scales of Eqs. (3) are (4) are used, and a dimensionless temperature is defined such that $\Theta = (T - T_s)/(T_\infty - T_s)$, where T_∞ is the temperature at the plasma torch exit ($z = L$), and T_s is the substrate temperature. The dimensionless energy equation is then

$$\tilde{u}\frac{\partial\Theta}{\partial\tilde{r}} + \tilde{w}\frac{\partial\Theta}{\partial\tilde{x}} = \frac{1}{RePr}\left[\frac{1}{\tilde{r}}\frac{\partial}{\partial\tilde{r}}\left(\tilde{r}\frac{\partial\Theta}{\partial\tilde{r}}\right) + \frac{\partial^2\Theta}{\partial\tilde{x}^2}\right], \qquad (46)$$

where the Prandtl number is $Pr = \mu\hat{C}_p/k$.

For a fluid undergoing uniform stagnation flow, the similarity supposition is that the temperature profile does not change shape at different values of r, that is, $\Theta = \Theta(\tilde{x})$.[21] Utilizing this assumption, Eq. (46) becomes

$$\tilde{w}\frac{d\Theta}{d\tilde{x}} = \frac{1}{RePr}\frac{d^2\Theta}{d\tilde{x}^2}. \qquad (47)$$

For finite Pr, as $Re \to \infty$ this equation simplifies to

$$\tilde{w}\frac{d\Theta}{d\tilde{x}} = 0, \qquad (48)$$

which has the solution $\Theta = 1$. Thus, in the region where the flow is nearly inviscid, the temperature is predicted to be constant, consistent with the full numerical result shown in Fig. 3. To correctly capture the actual temperature drop through the thermal boundary layer, it is necessary to rescale Eq. (47) using the same stretching as for the momentum equations, namely $X = Re^{1/2}\tilde{x}$ and $W = Re^{1/2}\tilde{w}$. The resulting boundary-layer equation is

$$W\frac{d\Theta}{dX} = \frac{1}{Pr}\frac{d^2\Theta}{dX^2}. \qquad (49)$$

Before implementing the Karman–Pohlhausen method, an approximate expression is selected for the temperature profile in the boundary layer

$$\Theta = a + b\xi_T + c\xi_T^2 + d\xi_T^3, \qquad (50)$$

where $\xi_T = X/\zeta_T$ and ξ_T is the dimensionless thermal boundary-layer thickness, related to the dimensional boundary-layer thickness by $\zeta_T = Re^{1/2}\delta_T/L$. The constraints imposed on the dimensionless temperature in the boundary layer are

$$\Theta = 0, \quad \frac{d^2\Theta}{d\xi_T^2} = 0, \qquad \text{at } \xi_T = 0, \qquad (51)$$
$$\Theta = 1, \quad \frac{d\Theta}{d\xi_T} = 0, \qquad \text{at } \xi_T = 1. \qquad (52)$$

Upon evaluation of the constants in Eq. (50), the dimensionless temperature profile becomes

$$\Theta = \frac{1}{2}\xi_T(3 - \xi_T^2). \qquad (53)$$

Because the relative thickness of the boundary layers, δ/δ_T, is a function of Pr, two different cases must be considered, depending on whether the thermal boundary layer is thinner or thicker than the momentum boundary layer.

A. $\delta_T < \delta$

For this case, viscous diffusion is stronger than thermal diffusion, and $\delta_T < \delta$. Energy transport within the thermal boundary layer occurs by both conduction and convection, and the velocity experienced by the fluid is that given by the expressions for $\hat{u}_{BL}$ and W from the previous section. Integrating Eq. (49) across the thermal boundary-layer yields the integral equation

$$-\frac{1}{Pr}\left.\frac{d\Theta}{dX}\right|_{X=0} = \int_0^{\zeta_T} W_{BL}\frac{d\Theta}{dX}\,dX. \qquad (54)$$

Substituting Eqs. (36) and (53) into Eq. (54) results in a quintic equation for ζ_T:

$$\zeta_T^5 - 14\zeta^2\zeta_T^3 = -\frac{17.5}{Pr}\zeta^3[4 + Re^{-1/2}\zeta], \qquad (55)$$

which must be solved numerically.

B. $\delta_T > \delta$

For this case, viscous diffusion is weaker than thermal diffusion, and $\delta_T > \delta$. The fluid within the thermal boundary layer experiences not only the velocity field characteristic of the momentum boundary layer, but also that from the potential flow field. While the upper portion of the thermal boundary layer is under the influence of the potential flow field, this comprises a relatively small fraction of the total thermal boundary-layer thickness because Pr is finite, and in fact, for gases it is $O(1)$. Nevertheless, when an integral equation identical to Eq. (54) is constructed, the limits of integration are separated so that the different velocity fields are taken into account:

$$-\frac{1}{Pr}\frac{d\Theta}{dX}\bigg|_{X=0} = \int_0^{\zeta} W_{BL}\frac{d\Theta}{dX}\,dX + \int_{\zeta}^{\zeta_T} W_{FS}\frac{d\Theta}{dX}\,dX\,. \tag{56}$$

Substituting Eqs. (34), (36), and (53) into Eq. (56) yields a polynomial expression for ζ_T:

$$\begin{aligned}\zeta_T^5 &- 3.75Re^{1/2}\zeta_T^4 + (1.25\zeta + 3.75Re^{1/2})\zeta\zeta_T^3 \\ &- [\zeta^3 + (1.5Re^{1/2} + 1.875Re^{-1/2}Pr^{-1})\zeta^2 \\ &+ 5.625Pr^{-1}\zeta - 7.5Re^{1/2}Pr^{-1}]\zeta_T^2 \\ &+ 0.143\zeta^5 + 0.107Re^{1/2}\zeta^4 = 0\,.\end{aligned} \tag{57}$$

V. DISCUSSION

As a simple illustration of the results obtained above, the effects of pressure and average temperature on boundary-layer thickness are investigated for conditions representative of those found in diamond arcjet reactors. In the system under study, pure H_2 is fed into the plasma torch where it encounters a high temperature plasma arc. Due to nonuniform mixing in the torch and extremely short residence times, only a fraction of the hydrogen dissociates into the atomic state. The H, H_2 mixture leaving the torch is mixed with CH_4, and the mole fractions of CH_4, H, and H_2 at the point of mixing are assumed to be 0.01, 0.2, and 0.79. Although the average velocity of the mixture at the torch exit depends not only on the hydrogen flow rate but also on the gas temperature and reactor pressure, a characteristic value of $U_\infty = 2 \times 10^5$ cm/s is used for all cases considered below. The separation distance between the torch exit and the substrate is assumed to be 15 cm. The predicted values of δ and δ_T will be compared to the full numerical solution of the governing equations, using the stagnation flow code SPIN.[24] The thermal boundary-layer thickness in the SPIN result is taken to be the point at which the temperature drops to 99% of its free stream value; the momentum boundary-layer thickness is the point where $\hat{u}$ is maximum.

A. Effect of temperature on boundary-layer thickness

To examine the dependence of boundary-layer thickness on effective temperature, calculations were carried out for $1000 \leqslant T_{\rm eff} \leqslant 2500$ K, at a single reactor pressure of 20 Torr. Thermophysical and multicomponent transport properties were evaluated using the Chemkin software library.[29,30] For this gaseous system, under the conditions considered the thermal boundary layer is thicker than the momentum boundary layer, and Eq. (57) is used to compute δ_T. [However, as illustrated in Fig. 5, the region over which $W_{BL} \approx W_{FS}$ is comparable in magnitude to ζ, and Eqs. (54) and (55) yield values of ζ_T very close to those predicted by Eq. (57).] Values for momentum and thermal boundary-layer thickness are plotted in Fig. 6 as functions of $T_{\rm eff}$. The solid symbols are the predictions resulting from Eqs. (41) and (57), while the open symbols are the values extracted from the SPIN calculations. It was not possible to specify "realistic" combinations of T_s and T_∞ in SPIN for $T_{\rm eff} <$ 1300 K or $T_{\rm eff} >$ 2200 K.

For the results in Eqs. (41) and (55), simple kinetic theory predicts that δ, $\delta_T \propto T^{3/4}$, which is very close to the behavior found in Fig. 6 for both the approximate re-

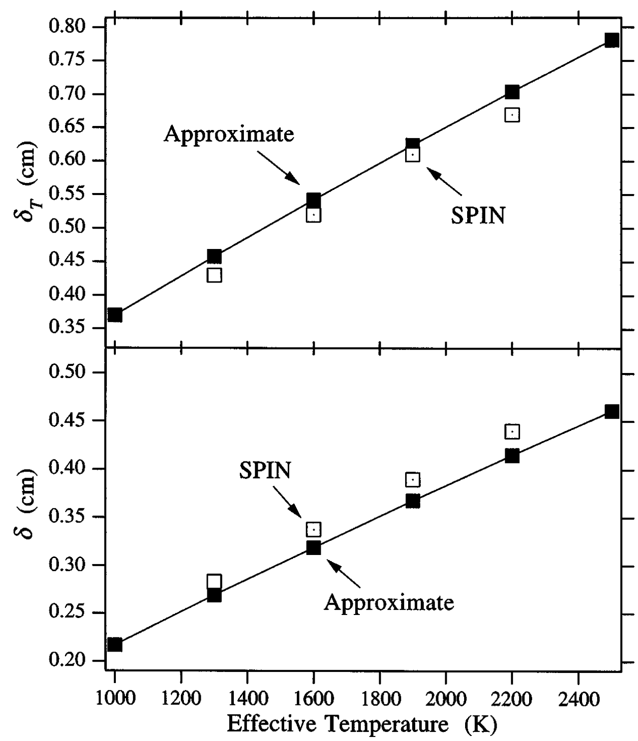

FIG. 6. The momentum and thermal boundary-layer thickness as functions of effective temperature for p = 20 Torr and $U_\infty = 2 \times 10^5$ cm/s. The closed symbols (■) are from the results of the present work, while the open symbols (□) are taken from numerical results of the governing conservation equations.[24]

sults and the SPIN calculations. The maximum difference between SPIN and the approximate results for $1300 \leqslant T_{\text{eff}} \leqslant 2200$ K is 6%.

B. Effect of pressure on boundary-layer thickness

To illustrate dependence of boundary-layer thickness on pressure, calculations were performed for $5 \leqslant p \leqslant 100$ Torr, with $T_s = 1200$ K and $T_\infty = 2500$ K ($T_{\text{eff}} = 1850$ K). This pressure range is characteristic of that used in reactors operating under subsonic conditions. Again, since $\delta_T > \delta$, Eq. (57) is used. Results for the momentum and thermal boundary-layer thickness as functions of p are plotted in Fig. 7; the values computed using Eqs. (41) and (57) are denoted by the solid symbols, while the SPIN results correspond to the open symbols.

C. Summary

Approximate expressions have been derived for the momentum and thermal boundary-layer thickness in forced convection, uniform stagnation flow. The results presented above are valid for conditions where $Re \gg 1$, and effects arising from flow swirl or disk rotation are negligible compared to the imposed stagnation flow. The expressions resulting from application of the Karman–Pohlhausen method are in very good qualitative and quantitative agreement with numerical solutions of the equations of motion and the thermal energy equation.

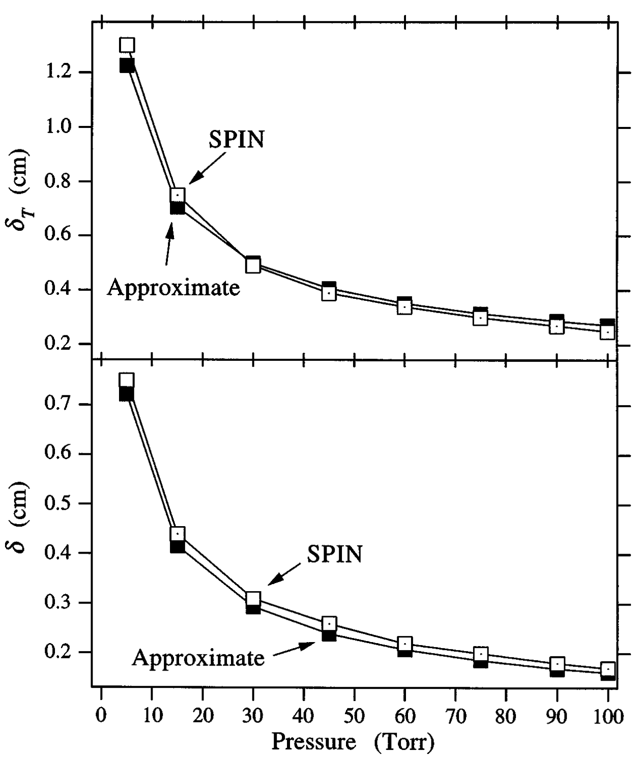

FIG. 7. The momentum and thermal boundary-layer thickness as functions of pressure for $T_s = 1200$ K, $T_\infty = 2500$ K, and $U_\infty = 2 \times 10^5$ cm/s. The closed symbols (■) are from the results of the present work, while the open symbols (□) are taken from numerical results of the governing conservation equations.[24]

ACKNOWLEDGMENTS

This work has been supported by the Materials Science Program at DARPA, Contract N00014-93-1-2002. J. Y. would like to thank Te-Hsin Wu for assistance in deriving the thermal boundary-layer expression.

REFERENCES

1. F. G. Celii and J. E. Butler, Ann. Rev. Phys. Chem. **42**, 643 (1991).
2. M. E. Coltrin and D. S. Dandy, J. Appl. Phys. **74**, 5803 (1993).
3. G. A. Raiche, G. P. Smith, and J. B. Jeffries, in *New Diamond Science and Technology,* edited by R. Messier, and J. T. Glass, J. E. Butler, and R. Roy (Mater. Res. Soc. Int. Symp. Proc. **NDST-2**, Pittsburgh, PA, 1991), p. 251.
4. D. G. Goodwin, Appl. Phys. Lett. **59**, 277 (1991).
5. N. Koshino, K. Kurihara, M. Kawarada, and K. Sasaki, in *Diamond and Diamond-Like Materials Synthesis,* edited by G. H. Johnson, A. R. Badzian, and M. W. Geis (Mater. Res. Soc. Symp. Proc. **EA-15**, Pittsburgh, PA, 1988), pp. 95–98.
6. S. Matsumoto, in *Diamond and Diamond-Like Materials Synthesis,* edited by G. H. Johnson, A. R. Badzian, and M. W. Geis (Mater. Res. Soc. Symp. Proc. **EA-15**, Pittsburgh, PA, 1988), pp. 119–122.
7. N. Ohtake, H. Tokura, Y. Kuriyama, Y. Mashimo, and M. Yoshikawa, *Proceedings of the First International Conference on Diamond and Diamond-Like Films,* edited by J. P. Dismukes (The Electrochemical Society, Pennington, NJ, 1989), pp. 93–105.
8. K. R. Stalder and R. L. Sharpless, J. Appl. Phys. **68**, 6187 (1990).
9. F. M. Cerio and W. A. Weimer, Rev. Sci. Instrum. **63**, 2065 (1992).
10. R. L. Woodin, L. K. Bigelow, and G. L. Cann, *Proceedings of Applications of Diamond Films and Related Materials* (Auburn, AL, 1991), p. 439.
11. L. Rongzhi, S. Hailiang, Y. Zhen, T. Sen, and Z. Hesun, *Proceedings of Applications of Diamond Films and Related Materials* (Auburn, AL, 1991), p. 207.
12. D. S. Dandy and M. E. Coltrin, J. Mater. Res. **10**, 1993 (1995).
13. B. W. Yu and S. L. Girshick, J. Appl. Phys. **75**, 3914 (1994).
14. D. G. Goodwin and G. G. Gavillet, J. Appl. Phys. **68**, 6393 (1990).
15. D. G. Goodwin, J. Appl. Phys. **74**, 6895 (1993).
16. L. K. Bigelow, N. M. Henderson, and R. L. Woodin, in *New Diamond Science and Technology,* edited by R. Messier, J. T. Glass, J. E. Butler, and R. Roy (Mater. Res. Soc. Int. Symp. Proc. **NDST-2**, Pittsburgh, PA, 1991), p. 529.
17. T. von Karman, Z. Angew, Math. Mech. **1**, 233 (1921).
18. W. G. Cochran, Proc. Cambridge Philos. Soc. **30**, 365 (1934).
19. U. T. Bödewadt, Z. Angew. Math. Mech. **20**, 241 (1940).
20. M. H. Rogers and G. N. Lance, J. Fluid Mech. **7**, 617 (1960).
21. E. M. Sparrow and J. L. Gregg, J. Heat Transfer **82**, 294 (1960).
22. G. H. Evans and R. Greif, Numer. Heat Transfer **14**, 373 (1988).
23. M. E. Coltrin, R. J. Kee, and G. H. Evans, J. Electrochem. Soc. **136**, 819 (1989).
24. M. E. Coltrin, R. J. Kee, G. H. Evans, E. Meeks, D. S. Dandy, F. M. Rupley, and J. F. Grcar, Sandia National Laboratories Report, SAND 91-8003 (1991).

25. J. F. Grcar, Sandia National Laboratories Report, SAND 91-8230 (1991).
26. J. F. Grcar, R. J. Kee, M. D. Smooke, and J. A. Miller, in *Twenty-First Symposium (International) on Combustion* (The Combustion Institute, Pittsburgh, PA, 1987), p. 1773.
27. K. Suzuki, A. Sawabe, and T. Inuzuka, Jpn. J. Appl. Phys. **29**, 153 (1990).
28. F. Zhang, Y. Zhang, Y. Yang, G. Chen, and X. Jiang, Appl. Phys. Lett. **57**, 1467 (1990).
29. R. J. Kee, F. M. Rupley, and J. A. Miller, Sandia National Laboratories Report, SAND89-8009B (1993).
30. R. J. Kee, G. Dixon-Lewis, J. Warnatz, M. E. Coltrin, and J. A. Miller, Sandia National Laboratories Report, SAND 86-8246 (1986).